Journal of Manufacturing Processes 79 (2022) 759–766

Contents lists available at ScienceDirect

Journal of Manufacturing Processes

journal homepage: www.elsevier.com/locate/manpro

Lightweight injection mold using additively manufactured Ti-6Al-4V lattice structures

Seong Je Park [a,b], Jun Hak Lee [a,b], Jeongho Yang [a,c], Woongbeom Heogh [a], Dongseok Kang [a], Si Mo Yeon [a], Sang Hoon Kim [a], Sukjoon Hong [b], Yong Son [a], Jiyong Park [a,d,*]

[a] Advanced Joining and Additive Manufacturing R&D Department, Korea Institute of Industrial Technology, 113-58 Seohaean-ro, Siheung, Gyeonggi-do 15014, Republic of Korea

[b] Optical Nanoprocessing Lab, Department of Mechanical Engineering, Hanyang University, 55 Hanyangdaehak-ro, Sangnok-gu, Ansan, Gyeonggi-do 15588, Republic of Korea

[c] School of Mechanical Engineering, Pusan National University, 2 Busandaehak-ro 63 beon-gil, Busan 46241, Republic of Korea

[d] Department of Convergence Manufacturing System Engineering, University of Science and Technology (UST), 217 Gajeong-ro, Yuseong-gu, Daejeon 34113, Republic of Korea

ARTICLE INFO

Keywords:
Lightweight injection mold
Lattice structure
Design for additive manufacturing (DfAM)

ABSTRACT

Injection mold requires a large weight, significant cost of material, safety management, and installation of auxiliary facilities. In this study, we realized a lightweight injection mold consisting of lattice structures through the additive manufacturing (AM) technology for overcoming these limitations. A compression test was conducted to understand the intrinsic mechanical properties of lattice structures according to density. Moreover, the external force applied to a mold using computer-aided engineering (CAE) was confirmed. Based on the results of the compression test of the lattice structure and CAE analysis for the mold, a lightweight injection mold was designed and fabricated to facilitate design for additive manufacturing. Furthermore, the lightweight injection mold was assembled into the injection machine and the injection test was performed. The weight and amount of material of the mold were reduced by ~79%, and the injection molding of 400 shots was successful using polyvinyl chloride (PVC) without damaging the mold.

1. Introduction

In various industries, the lightweightness is closely related to fuel efficiency improvement and low safety-related risks [1,2]. From this perspective, this study focuses on the mold-based industry. In particular, large molds are needed to manufacture parts in the automobile, aerospace, ship and home appliances industries [3–7]. However, the large injection molds have issues associated with the weight and unit cost of mold material, the risk of safety management, and the demand for auxiliary facilities, due to repeated removal and movement of equipment for design changes [8]. These issues can be overcome by using lightweight molds. In other words, if the interior of the mold manufactured by the AM technology have a porous structure, the mold will be efficient in terms of being lightweight.

To reduce the weight of the mold, a polymer rather than a metal is the preferred mold material. The early attempt of injection mold production via AM technology and polymer used the materials extrusion (ME) type because the AM type is easy to access and can utilize various thermoplastic materials. Approximately 40 shots were injected using acrylonitrile butadiene styrene (ABS) and low density polyethylene (LDPE) [9]. A mold was also fabricated using polyetheretherketone (PEEK), a super engineering plastic, and more than 110 shots were injected without damaging the PEEK molds [10]. However, because the ME type was used, the quality of the injection parts was low, and there was a risk of leakage due to the unique deposition mechanism (layer-by-layer) imparted during the ME [11,12]. Moreover, injection molds were prepared through vat photopolymerization (VP) 3D printing technologies such as digital light processing (DLP) and stereolithography (SLA). By exploiting the advantages of the VP-type polymer molds, micro-injection molding of thin cavities was implemented [13]. Attempts were also devoted toward the injection molding of polyethylene (PE) under 100 shots and polyoxymethylene (POM) under 55 shots [14].

* Corresponding author at: Advanced Joining and Additive Manufacturing R&D Department, Korea Institute of Industrial Technology, 113-58 Seohaean-ro, Siheung, Gyeonggi-do 15014, Republic of Korea.
E-mail address: j.park@kitech.re.kr (J. Park).

https://doi.org/10.1016/j.jmapro.2022.05.022
Received 30 December 2021; Received in revised form 6 April 2022; Accepted 4 May 2022
Available online 23 May 2022

Although the VP-type polymer molds do not exhibit surface defect formation and suffer from leakage unlike the ME-type polymer molds, they still have the disadvantage of low thermal properties [15–18]. Thus, for lightweight injection molds, polymer molds are ideal; however, they have limitations such as low thermal resistance.

Polymer injection molds with low thermal resistance have been replaced by metal ones manufactured using lattice structures in attempting to increase the thermal property. The metal mold is fabricated through a powder bed fusion (PBF) process, as this technique impart high thermal resistance [19,20]. In general, there are many processes such as design, milling, lathe, drilling, wire cutting, computer numerical control (CNC) machining, and assembly are needed to manufacture a traditional mold with skilled labor at all stages thereof, [21] while AM technology can simply reduce the process such as design, AM, and assembly. In this process, the costs of manufacturing can be saved, even material costs by using lattice structures. Using AM technologies, the previous researchers only investigated the maximum loads that the lattice can withstand and the formation of minimal surface structures through computer-aided engineering (CAE) for the fabrication of lightweight molds. There have also been a few studies on component-level applications [21,22]. In particular, it is difficult to find research for large-scale manufacturing fields, such as injection molding. Thus, comprehensive research is needed, including that based on the identification of the mechanical properties of lightweight structures as well as manufacture of lightweight molds via AM technology and their applicability for injection molding.

Herein, a comprehensive study was performed, including compression tests of lattice structures, CAE analysis of molds for design for additive manufacturing (DfAM), AM of lightweight molds, and feasibility test for injection molding. For stretch-and bending-dominant lattice structures, yield strength was first investigated in terms of the compression load applied to the injection mold. In addition, the stress distribution of the mold was confirmed through CAE analysis, considering the clamping force and pressure of the polymer material in the mold during injection. Based on compression test and CAE analysis, each lattice structure capable of resisting the load that occurred during injection molding was appropriately placed inside the mold. Lightweight molds were additively fabricated using the Ti-6Al-4V which is required for polyvinyl chloride (PVC) or rubber injection; mold materials undergo corrosion based on chloride and sulfur [23–25].

As a results, the weight was successfully reduced by ~79% compared to that of the solid mold, and 400 shots using PVC were injected in the lightweight molds without any damage, which confirmed the feasibility of the lightweight molds for injection molding. In other words, we demonstrated a lightweight mold with lattice structures that can be used in the field by applying AM technology with Ti-6Al-4V, which is well known for its excellent mechanical properties and lightness but is difficult to cut [26,27]. Thus, it is expected to contribute to expanding the application field using AM technologies in the mold industry including safety-related risks prevention and cost reduction.

2. Experimental setup

2.1. Materials and machine

Ti-6Al-4V powder (LaserForm Ti Gr23, 3D Systems, USA) was used in a commercially available PBF system (DMP flex 350, 3D Systems, USA). The yield strength and elastic modulus in compression load of additively manufactured solid structure is 1563 MPa and 3.7 GPa. The morphology of the Ti-6Al-4V powder particles was measured through scanning electron microscopy (SEM; JSM-5800, JEOL, Japan). The Ti-6Al-4V powder was composed of titanium (Ti), aluminum (Al), and vanadium (V), which had a mean particle size of 33 μm, as measured using a laser scattering particle size distribution analyzer (Partica LA-960, Horiba, Japan). The morphology and, size distribution of the powder particles are shown in Fig. 1. The composition of powder and AM parts are shown in Table 1. Al, V, Fe, C and H had insignificant changing in powder and AM parts. The AM part reacted with O and N in the atmosphere during processing, increasing the composition.

2.2. Design and identify mechanical properties of lattice structures

The lattice structures are roughly classified into two types, according to Maxwell's stability criterion shown in Eq. (1) in three dimensional structures: [28].

$$M = b - 3j + 6 \tag{1}$$

Where b is the number of struts and j is the joint. $M \geq 0$ indicates a stretch-dominant lattice structure, whereas $M < 0$ represents a bending-dominant structure, as shown in Fig. 2 [29]. In this study, the lattice structures were used as octet-truss (OT) and diamond (DM), as shown Fig. 3(a), followed by ISO 13314: Mechanical testing of metals – Ductility testing – Compression test for porous and cellular metals [30]. OT was chosen as the stretch-dominant structure. The OT has the most struts in the unit cell compared to any other lattice structure [31]. DM was chosen as the bending-dominant structure, which has superior energy absorption upon the application of the compression load [32]. All lattice structures consist of OT and DM, according to density, such as 10%, 30%, and 50%. In generally, the density is defined by Eq. (2):

$$\rho = \rho_l/\rho_s \tag{2}$$

Table 1
Composition of powder and AM part.

Composition	Powder (%)	AM part (%)
Aluminum (Al)	6.48	6.47
Vanadium (V)	3.87	3.94
Iron (Fe)	0.19	0.20
Carbon (C)	0.02	0.03
Oxygen (O)	0.11	0.13
Nitrogen (N)	0.001	0.008
Hydrogen (H)	0.002	0.003

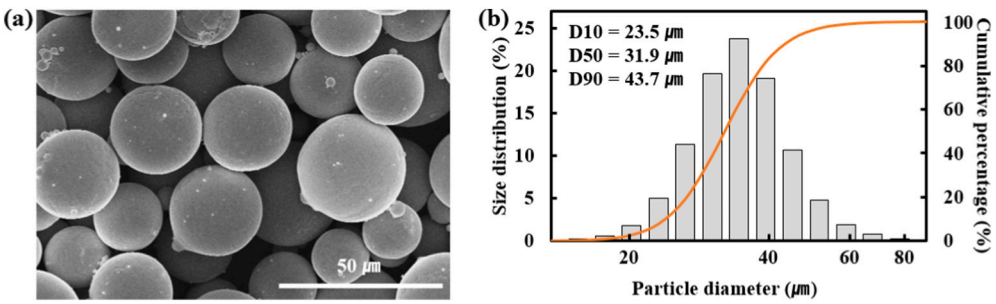

Fig. 1. (a) Powder morphology and (b) size distribution of Ti-6Al-4V powder.

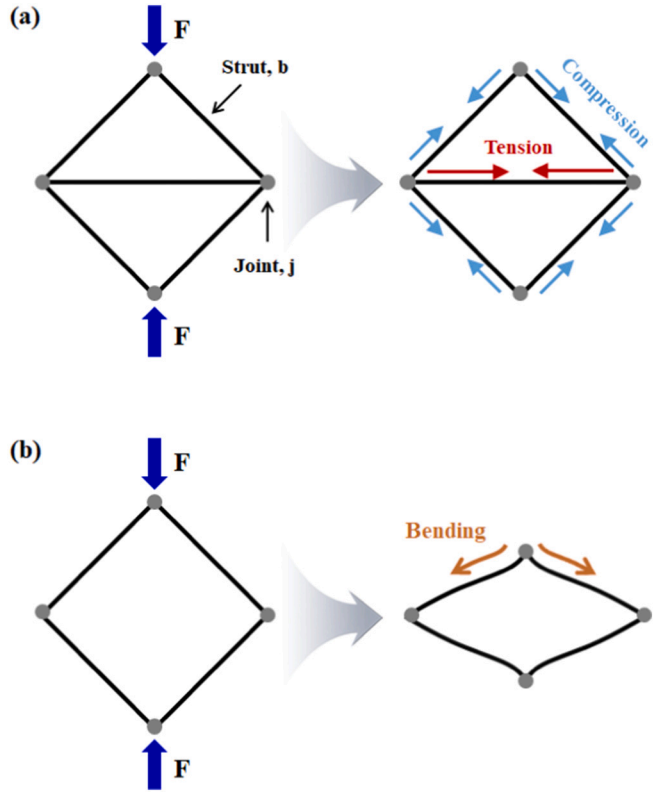

Fig. 2. (a) Stretch-dominant structure having M ≥ 0 and (b) bending dominant structure having M < 0.

where ρ_l is the density of the lattice structures and ρ_s that of the solid of which it is made [33]. In this study, the density was designated as a set value in the software. Thus, the density is controlled by the thickness of the struts in unit cells of the same size. A solid with a thickness of 3 mm was fabricated on the top and bottom of the lattice structures because our application, the mold, is a solid shape on the surface for the quality of injection parts, as shown Fig. 3(b). The lattice structures were designed using 3DXpert (3D systems, U. S. A.), and consisted of a 1 × 1 × 1 mm unit cell in the compression specimens. The laser power, scan speed, layer thickness, and hatching distance for fabricating the lattice and solid structures were set according to the manufacturer's recommended values listed in Table 2.

The compression specimens were set on a universal testing machine (AGS-X 300kN, Shimadzu, Japan). The compression test was performed at a crosshead speed of 2 mm/min. All tests were performed by applying lubricants at top and bottom to minimize friction and on three specimens. All quantitative results, such as yield strength and energy absorption during the compression test, are displayed as the mean ± standard deviation.

2.3. CAE analysis

The structural analysis was performed to confirm the stress distribution of unit cells of lattice structures in compression load according to density and mold during injection molding using software of ANSYS (ANSYS Inc., USA) static structural. In case of structural analysis of the unit cell, the mesh size was set to 0.2 mm. The displacement of 0.01 mm was applied as a boundary condition at the top of the unit cell model to assume the load under compression. The injection mold carried out a structural analysis to design the inside of the mold as lattice structures according to the stress distribution. In the mold analysis, the mesh size was performed as a value of default. The boundary condition in the mold was set to 50 MPa for the part filled with material and 37.5 kN for the other part.

2.4. Injection molding test

To verify the feasibility of the additively manufactured lightweight mold with the Ti-6Al-4V lattice structure, the mold set was equipped with an injection molding machine (MJ5700, Dongsin, Republic of Korea). The PVC melt was injected into a lightweight mold. The injection nozzle temperature, screw speed, packing pressure, and cooling time were set to 250 °C, 20 mm/s, 22 MPa, and 15 s, respectively. The molds were designed with a pair of ring shapes. The injection molding test was conducted repeatedly until injection cycles reached 400 shot.

3. Results and discussion

3.1. Compression behavior of lattice structures

Fig. 4(a) represents the photographs of whole and optical microscope image of a part for specimens. The strut diameter of OT has approximately 0.15, 0.21, and 0.28 mm when the density is 10, 30, and 50%, respectively. The DM's strut diameter has approximately 0.3, 0.4, and 0.5 mm when the density is 10, 30, and 50%, respectively. Fig. 4(c) shows the specimens after the compression tests. All compression specimens were fractured with a slip plane inclined by 45° with respect to the horizontal plane, as shown in Fig. 4(b). These failure modes occurred at the macro level because the maximum shear stress was applied at 45° in the compression load direction [34]. This macro-level failure mode has been reported in the literature [35]. Fig. 4(c) shows the stress–strain curve for the compression tests of OT and DM lattice structures with densities of 10%, 30%, and 50%. In general, the stretch-dominant lattice structures show the oscillation behavior after achieving

Table 2
Fabrication conditions of the lattice and solid structures.

Process parameter	Lattice structures	Solid structures
Laser power (W)	125	145
Laser scan speed (mm/s)	2800	1000
Layer thickness (μm)	30	30
Hatching distance (μm)	110	82

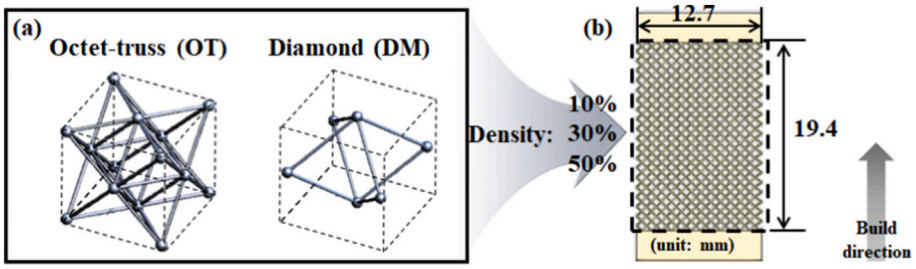

Fig. 3. Design of lattice structures for (a) a unit cell and (b) compression specimens.

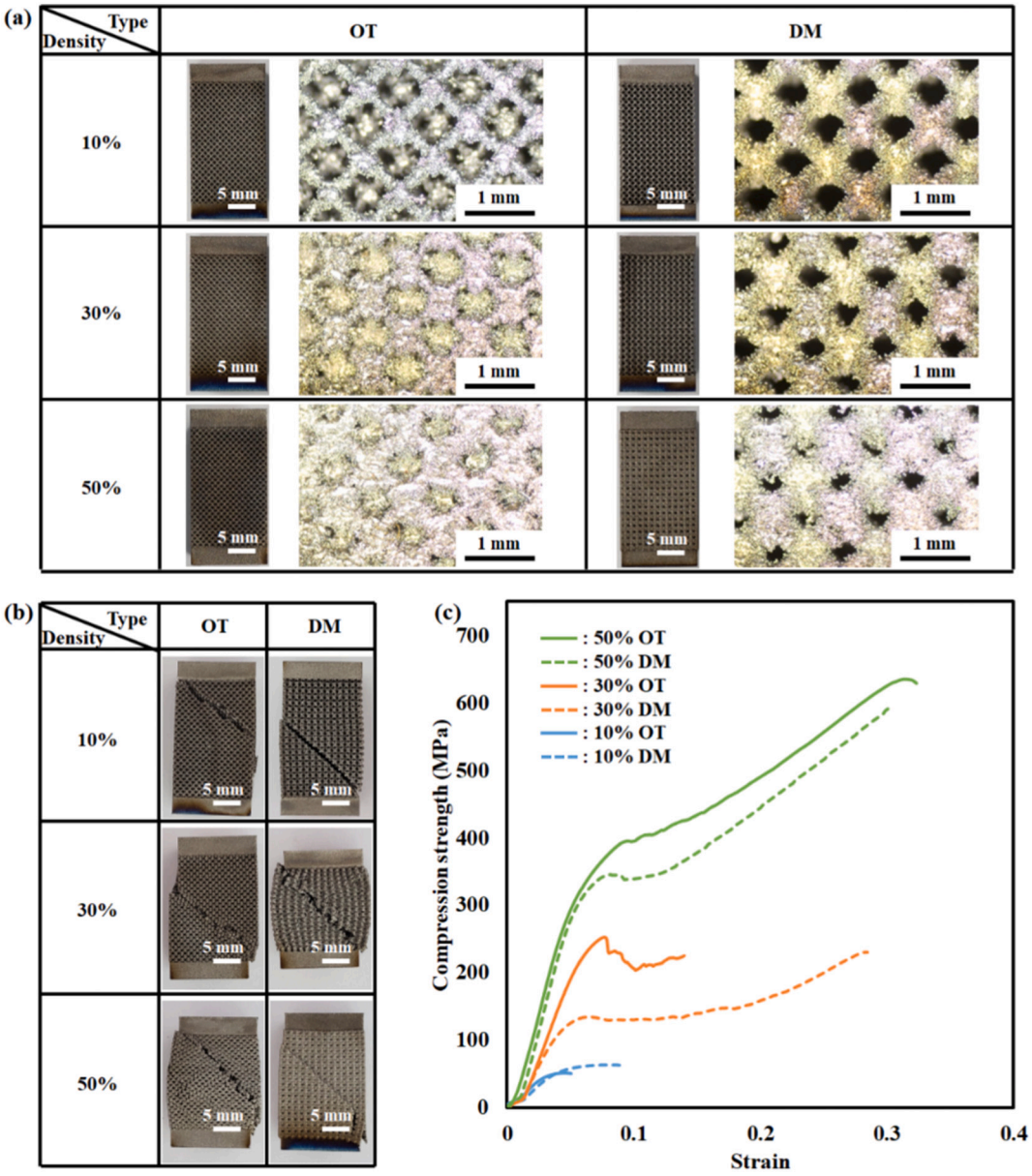

Fig. 4. (a) Photographs and optical microscope image of specimens. (b) Photographs of specimens after the compression test. (c) Stress–strain curve based on compression test results according to density.

the required yield strength because the struts break one by one under a compression load [32,36,37]. In contrast, the bending-dominant lattice structures show a long plateau stress behavior after achieving the required yield strength because the struts hold up without breaking under a compression load [38]. In this study, at all densities, the DM showed a longer plateau stress behavior than the OT because the DM has bending-dominant lattice structures. However, although the OT is a stretch-dominant lattice structure, it showed oscillation behavior after achieving the required yield strength at a density of only 30%. In particular, a high initial stress at the 250 MPa level was followed by an abrupt stress drop after achieving the required yield strength. The OT can carry high stress at small deformations owing to the fully constrained geometry, which leads to a higher modulus than that of DM. In the case of 50% density, it is similar to the behavior of a solid specimen rather than that of the lattice structures [39,40]. This is because the higher the density, the earlier the densification occurs, which induced that specimens had become more brittle alike solid [41]. When the density is 10%, because of the strut thickness, the OT cannot withstand the compression load, and brittle fracture occurs collectively.

3.2. Comparison of compression test results

Generally, in the case of the compression tests, the ultimate compression strength is not clear because of the presence of densification in the ductility materials; therefore, it is often expressed in terms of yield strength [42]. Fig. 5(a) and (b) represent the yield strength and energy absorption for OT and DM with varying densities. The yield strength is determined from the stress-strain curve depending on the method of 0.2% offset [43]. The energy absorption or toughness is calculated according to Eq. (3):

$$W = \int_0^{\varepsilon_m} \sigma d\varepsilon \tag{3}$$

where σ is the stress and ε is the strain. The energy absorption or toughness can be calculated by integrating the area under the stress-strain curve per unit volume for a specimen, up to a strain ε_m [44].

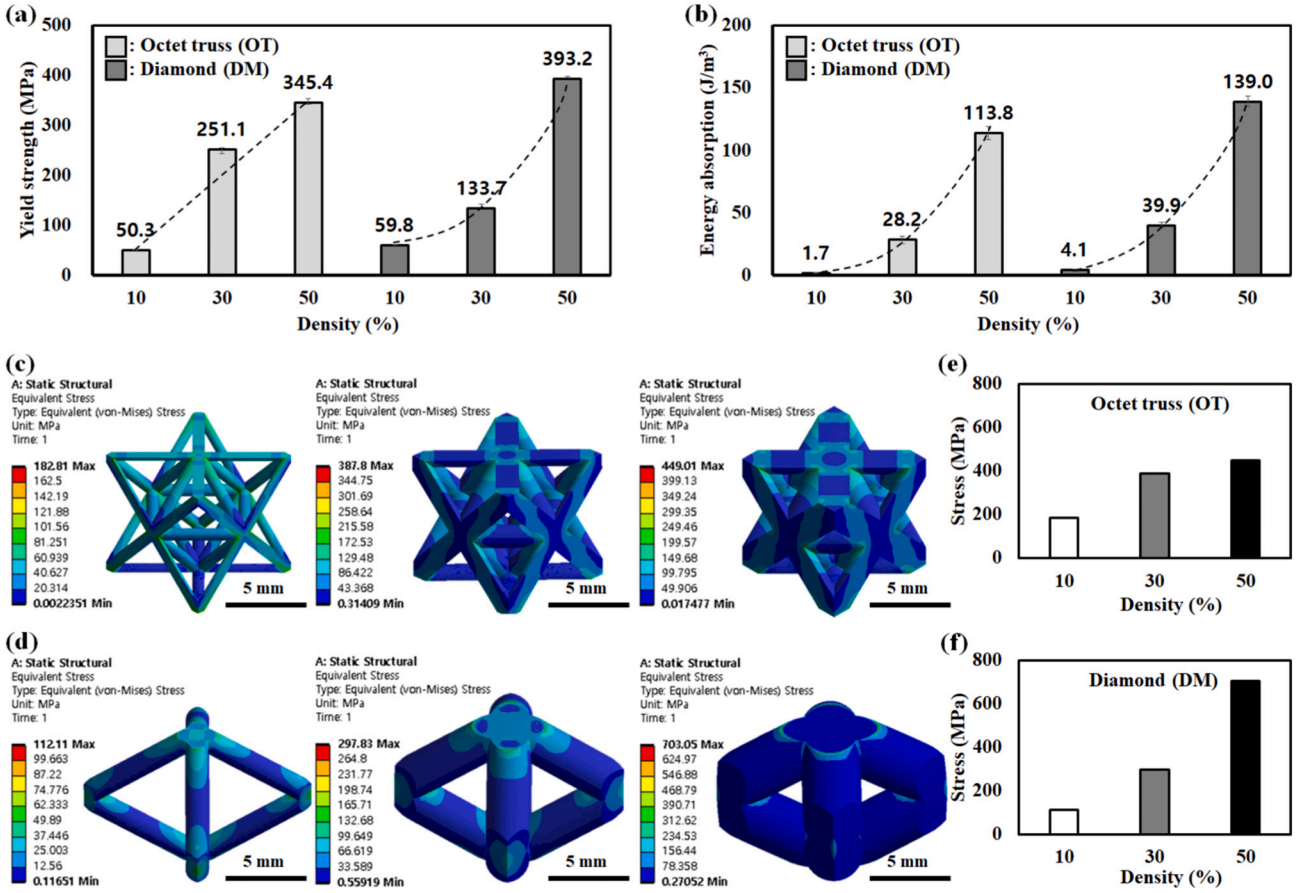

Fig. 5. Experimental results for (a) yield strength and (b) energy absorption with varying density for the compression tests of the OT and DM (mean ± standard deviation, n = 3). Results of structural analysis of the unit cell for the (c) OT at 10% (left), 30% (middle) and 50% (right) densities and (d) DM at 10% (left), 30% (middle) and 50% (right) densities. Maximum stress of the (e) OT and (f) DM in the structural analysis result as a function of density.

When the density is 10%, the OT and DM show similar yield strengths because fracture occurs before appearing the characteristics of stretch and bending dominant. The stretching and bending characteristics appeared at a density of 30%. The OT exhibits high resistance under the compression load, especially because of the interaction among many struts [36,45,46] In contrast, the DM is vulnerable to compression load because of its bending-dominant structures [47,48]. However, when the density was 50%, the DM exhibited the highest yield strength because the number of struts was small and the thickness of the struts was higher than that in the OT structures. This performance is attributed to the linear increase in the OT (yield strength = 7.3775 × density – 5.725 with R^2 = 0.96) and a quadratic increase in the DM yield strength (yield strength = 0.232 × density^2–5.585 × density + 92.45 with R^2 = 1) based on the following relationship between the elastic modulus and density as shown Eq. (4): [49].

$$(E/E_s) = C\,(\rho/\rho_s)^n \tag{4}$$

where E and E_s are the elastic modulus of the lattice structure and solid structure, respectively. The elastic modulus calculated from the linear region in resulting stress-strain curve before yield. The stretch- and bending-dominant structures generally have n values close to 1 and 2, respectively [50,51]. To demonstrate these experimental results in terms of yield strength, structural analysis was carried out at densities of 10%, 30%, and 50%. Fig. 5(c) and (d) show the structural analysis results according to the density of the unit cell of the OT and DM, respectively. Based on these structural analyses, the maximum stress of each result for the OT and DM is shown in Fig. 5(e) and (f). For the OT, the yield strength increased marginally from 30% to 50% density, whereas for the DM, the yield strength increased significantly. The tendencies observed through the experimental and structural analyses of the compression results were similar. The yield strength of the stretch-dominant structures (OT) increases linearly, whereas that of the bending-dominant structures (DM) exhibits a quadratic increase with density. In terms of energy absorption, the OT and DM show a quadratic increase with density, as shown in Fig. 5(b). The DM exhibits a higher energy absorption than the OT because bending-dominant structures have a superior strain, owing to a long plateau stress. The yield strength and energy absorption can be controlled over 50.3–393.2 MPa and 1.7–139.0 J/m^3, respectively.

3.3. CAE analysis for DfAM of injection mold

The yield strength of each lattice structure according to density is identified in Section 3.2. For placing the lattice structures inside the mold, DfAM was carried out to calculate the clamping force applied to the mold through CAE. The clamping force is expressed as the product of the projected area and the mean pressure of materials the inner mold [52]. PVC was selected as the injection material in this study. PVC have mean pressure of 50 MPa inner mold when injected [53]. The projected area in this mold was approximately 750 mm^2, as shown in Fig. 6(a). Thus, a maximum clamping force of 37.5 kN. Fig. 6(b) and (c) represent the boundary conditions for the PVC-filled areas and the other parts investigated in the structural analysis. In order to inject the shape selected in this study, the PVC-filled part is subjected to a maximum pressure of ~86.2 MPa, and the part that has to withstand the clamping force is subjected to a maximum pressure of ~10 MPa, as shown in Fig. 6 (d). Therefore, without considering the safety factor, it is concluded that

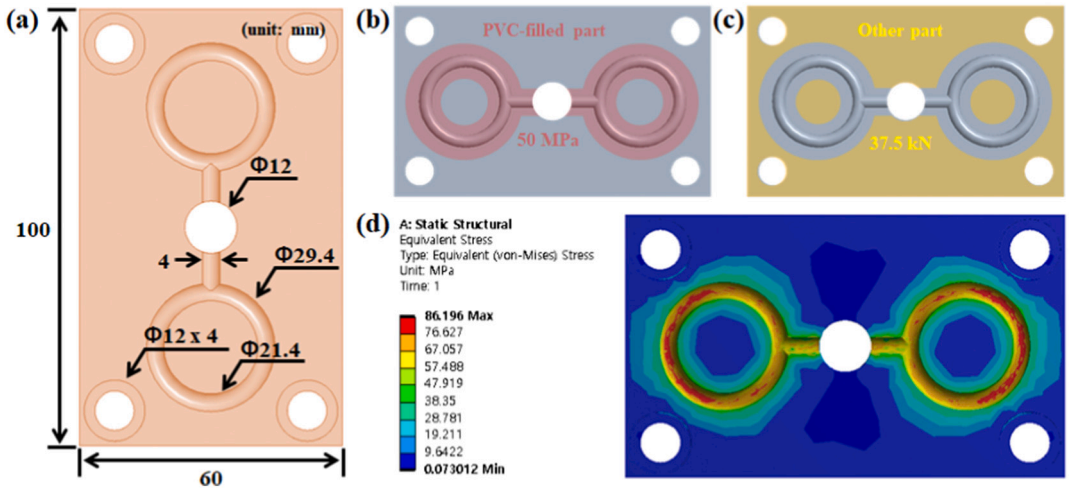

Fig. 6. (a) CAD modeling of the injection mold. Boundary conditions for (b) PVC-filled and (c) other part. (d) Results of structural analysis for stress distribution under injection condition.

the PVC-filled part and other part require a lattice structure with yield strengths of ≥86.2 MPa and ≥10 MPa, respectively.

3.4. AM of injection mold

Based on the results of the compression test and DfAM through CAE, the mold was additively manufactured as shown Fig. 7(a) by applying a safety factor of ≥2. Thus, the PVC-filled and other parts were designed and fabricated with 50% DM and10% OT, respectively, as shown in Fig. 7(b). In particular, the part of the PVC-filled area is designed as the bending-dominant structure having high energy absorption to easily absorb pressure of materials. The other part was designed as the stretch-dominant structure with a high elastic modulus to resist clamping force during the injection cycle. The top surface of mold was fabricated the solid. The solid and lattice molds in this study show a definite difference in terms of the mold weight. The lightweight mold fabricated in this study exhibited reduction in the weight and amount of materials of ~79% compared to the Ti-6Al-4V solid mold, as shown in Fig. 7(b).

3.5. Injection molding test of lightweight mold

If injection molding is not possible, it is not worth conducting for the fabrication of a lightweight injection mold. Therefore, to verify the applicability of lightweight molds, PVC was injected at a nozzle temperature of 250 °C into a lightweight mold via an injection machine, as shown in Fig. 8(a). As a result, the lightweight mold endured the clamping force and injection pressure applied during the injection cycle, including that the mold surface was clean as shown in Fig. 8(b), and 400 shots could be injected without damaging the lightweight mold, as shown in Fig. 8(c). The feasibility test results suggests that the

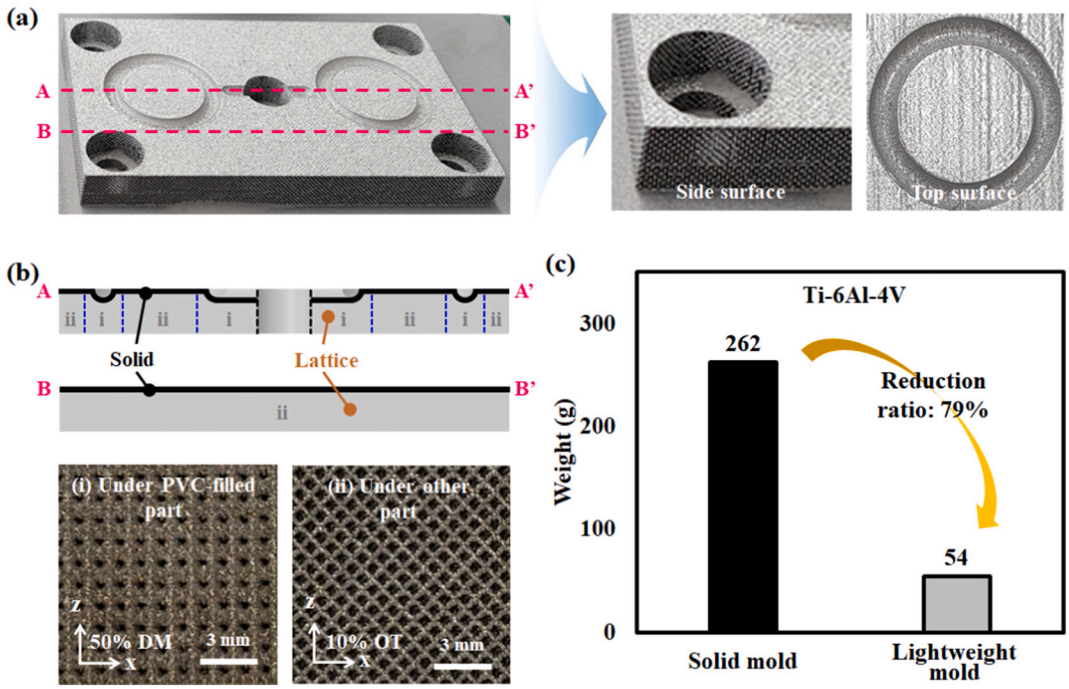

Fig. 7. (a) Photographs of additively manufactured mold. (b) Sectional view of step height the fabricated mold (along line A-A' and B-B' in (a)). (c) Comparison of weight between Ti-6Al-4V sold and lightweight molds.

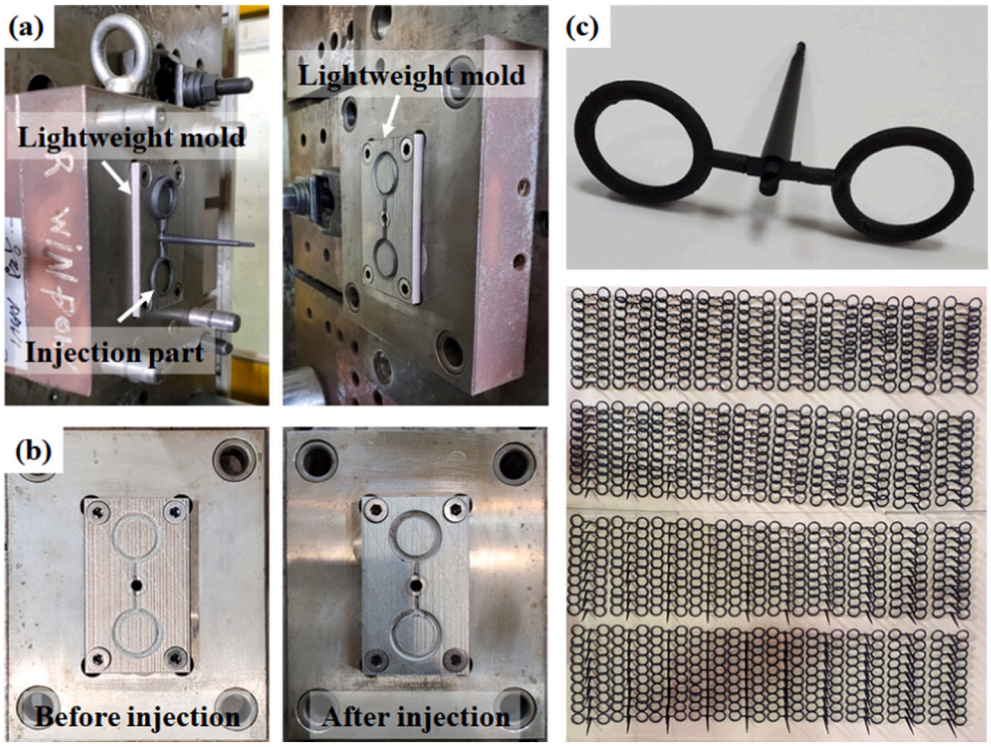

Fig. 8. (a) Photographs of the equipment of lightweight molds and injection part in the injection molding system. (b) Lightweight molds for cavity before (left) and after (right) 400 shots injection molding. (e) Injection parts using the lightweight mold.

lightweight molds could potentially be used in the large mold industry.

4. Conclusions

In various industries, lattice structures have been extensively used as lightweight materials that can be easily fabricated via AM rather than subtractive manufacturing. To exploit the benefits of the lattice structure lighter than solid within same volume, herein, the verification of the compression behavior of lattice structures such as OT and DM, structural analysis of target application, injection molding via CAE, 3D printing of the lightweight mold with placement of lattice structures, and injection testing for verifying feasibility of the lightweight mold were conducted. Approximately 79% reduction in the weight of the lightweight mold having lattice structures was successfully achieved, and 400 shots of PVC could be injected without any damage to the lightweight mold. Thus, the feasibility of the as-prepared lightweight mold for injection molding was confirmed. Thus, this study is believed to be an effective technology for many 3D printing or mold users.

Declaration of competing interest

The authors declare that they have no known competing financial interests or personal relationships that could have appeared to influence the work reported in this paper.

Acknowledgments

We thank Hyo Sin Park and No Chun Park, the co-president of Sung Won Tech., for technical issues about the experiments of injection molding. This study was supported by the Technology Innovation Program funded by the Ministry of Trade, Industry & Energy(MOTIE) of Korea (20010917, Development of automotive parts to improve driving performance and passenger convenience using DfAM based 3D printing manufacturing technology) and a KITECH internal project (EH210006, Establishment of the Rapid Manufacturing Platform for Ceramic Additive Manufacturing).

References

[1] Lambiase F, Scipioni SI, Lee CJ, Ko DC, Liu F. A state-of-the-art review on advanced joining processes for metal-composite and metal-polymer hybrid structures. Materials (Basel) 2021;14(8).
[2] Davies HC, Bastien C. An approach for the crash safety assessment of smaller and lightweight vehicles. Transp Policy 2021;105:12–21.
[3] Zhao Z, He X, Liu M, Liu B. Injection mold design and optimization of automotive panel. In: 2010 third international conference on information and computing; 2010. p. 119–22.
[4] Li X-P, Gong N-N, Guan Y-J, Cheng G-M. Thermal and stress analysis of rapid electric heating injection mold for a large LCD TV panel. Appl Therm Eng 2011;31 (17–18):3989–95.
[5] Choi JH, Choi SH, Park D, Park CH, Rhee BO, Choi DH. Design optimization of an injection mold for minimizing temperature deviation. Int J Automot Technol 2012; 13(2):273–7.
[6] Kuo C-C, Zhu Y-J, Wu Y-Z, You Z-Y. Development and application of a large injection mold with conformal cooling channels. Int J Adv Manuf Technol 2019; 103(1–4):689–701.
[7] Di Fratta C, Sun Y, Causse P, Trochu F. A dimensionless characteristic number for process selection and mold design in composites manufacturing: part II—applications. J Compos Sci 2020;4(1).
[8] Wei Z, Feng Y-X, Tan J-R, Wang J-L, Li Z-K. Multi-objective performance optimal design of large-scale injection molding machine. Int J Adv Manuf Technol 2008;41 (3–4):242–9.
[9] Masood SH, Song WQ. Development of new metal/polymer materials for rapid tooling using fused deposition modelling. Mater Des 2004;25(7):587–94.
[10] Park SJ, Lee JE, Park J, Lee N-K, Son Y, Park S-H. High-temperature 3D printing of polyetheretherketone products: perspective on industrial manufacturing applications of super engineering plastics. Mater Des 2021;211.
[11] Park SJ, Lee JE, Park JH, Lee NK, Lyu M-Y, Park K, Koo MS, Cho SH, Son Y, Park S-H. Enhanced solubility of the support in an FDM-based 3D printed structure using hydrogen peroxide under ultrasonication. Adv Mater Sci Eng 2018;2018:1–10.
[12] Lee JE, Park SJ, Yoon Y, Son Y, Park SH. Fabrication of 3D freeform porous tubular constructs with mechanical flexibility mimicking that of soft vascular tissue. J Mech Behav Biomed Mater 2019;91:193–201.
[13] Zhang Y, Pedersen DB, Gøtje AS, Mischkot M, Tosello G. A soft tooling process chain employing additive manufacturing for injection molding of a 3D component with micro pillars. J Manuf Process 2017;27:138–44.
[14] Surace R, Basile V, Bellantone V, Modica F, Fassi I. Micro injection molding of thin cavities using stereolithography for mold fabrication. Polymers (Basel) 2021;13 (11).

[15] Razavi Bazaz S, Rouhi O, Raoufi MA, Ejeian F, Asadnia M, Jin D, Ebrahimi Warkiani M. 3D printing of inertial microfluidic devices. Sci Rep 2020;10(1):5929.
[16] Gordeev EG, Galushko AS, Ananikov VP. Improvement of quality of 3D printed objects by elimination of microscopic structural defects in fused deposition modeling. PLoS One 2018;13(6):e0198370.
[17] Goo B, Hong C-H, Park K. 4D printing using anisotropic thermal deformation of 3D-printed thermoplastic parts. Mater Des 2020;188.
[18] Ji A, Zhang S, Bhagia S, Yoo CG, Ragauskas AJ. 3D printing of biomass-derived composites: application and characterization approaches. RSC Adv 2020;10(37): 21698–723.
[19] Tosto C, Tirillò J, Sarasini F, Cicala G. Hybrid Metal/Polymer filaments for fused filament fabrication (FFF) to print metal parts. Appl Sci 2021;11(4).
[20] Thompson Y, Gonzalez-Gutierrez J, Kukla C, Felfer P. Fused filament fabrication, debinding and sintering as a low cost additive manufacturing method of 316L stainless steel. Addit Manuf 2019;30.
[21] Malca C, Santos C, Sena M, Mateus A. Development of SLM cellular structures for injection molds manufacturing. Sci Technol Mater 2018;30(1):13–22.
[22] Wu T, Liu K, Tovar A. Multiphase topology optimization of lattice injection molds. Comput Struct 2017;192:71–82.
[23] Gurrappa I. Characterization of titanium alloy Ti-6Al-4V for chemical, marine and industrial applications. Mater Charact 2003;51(2–3):131–9.
[24] Cui C, Hu B, Zhao L, Liu S. Titanium alloy production technology, market prospects and industry development. Mater Des 2011;32(3):1684–91.
[25] Kaseem M, Choe H-C. Simultaneous improvement of corrosion resistance and bioactivity of a titanium alloy via wet and dry plasma treatments. J Alloys Compd 2021;851.
[26] Uhlmann E, Kersting R, Klein TB, Cruz MF, Borille AV. Additive manufacturing of titanium alloy for aircraft components. Procedia CIRP 2015;35:55–60.
[27] Pervaiz S, Rashid A, Deiab I, Nicolescu M. Influence of tool materials on machinability of titanium- and nickel-based alloys: a review. Mater Manuf Process 2014;29(3):219–52.
[28] Fleck NA, Deshpande VS, Ashby MF. Micro-architectured materials: past, present and future. Proc R Soc A: Math Phys Eng Sci 2010;466(2121):2495–516.
[29] Kang D, Park S, Son Y, Yeon S, Kim SH, Kim I. Multi-lattice inner structures for high-strength and light-weight in metal selective laser melting process. Mater Des 2019;175.
[30] Ghouse S, Babu S, Nai K, Hooper PA, Jeffers JRT. The influence of laser parameters, scanning strategies and material on the fatigue strength of a stochastic porous structure. Addit Manuf 2018;22:290–301.
[31] Kaur M, Yun TG, Han SM, Thomas EL, Kim WS. 3D printed stretching-dominated micro-trusses. Mater Des 2017;134:272–80.
[32] Maconachie T, Leary M, Lozanovski B, Zhang X, Qian M, Faruque O, Brandt M. SLM lattice structures: properties, performance, applications and challenges. Mater Des 2019;183.
[33] Ashby MF. The properties of foams and lattices. Philos Trans A Math Phys Eng Sci 2006;364(1838):15–30.
[34] Van Hooreweder B, Apers Y, Lietaert K, Kruth JP. Improving the fatigue performance of porous metallic biomaterials produced by selective laser melting. Acta Biomater 2017;47:193–202.
[35] Li SJ, Murr LE, Cheng XY, Zhang ZB, Hao YL, Yang R, Medina F, Wicker RB. Compression fatigue behavior of Ti–6Al–4V mesh arrays fabricated by electron beam melting. Acta Mater 2012;60(3):793–802.
[36] Wagner MA, Lumpe TS, Chen T, Shea K. Programmable, active lattice structures: unifying stretch-dominated and bending-dominated topologies. Extreme Mech Lett 2019;29.
[37] Sun ZP, Guo YB, Shim VPW. Characterisation and modeling of additively-manufactured polymeric hybrid lattice structures for energy absorption. Int J Mech Sci 2021;191.
[38] Park J-H, Park K. Compressive behavior of soft lattice structures and their application to functional compliance control. Addit Manuf 2020;33.
[39] Schulze C, Weinmann M, Schweigel C, Kessler O, Bader R. Mechanical properties of a newly additive manufactured implant material based on ti-42Nb. Materials (Basel) 2018;11(1).
[40] Ait-Mansour I, Kretzschmar N, Chekurov S, Salmi M, Rech J. Design-dependent shrinkage compensation modeling and mechanical property targeting of metal FFF. Prog Addit Manuf 2020;5(1):51–7.
[41] Choy SY, Sun C-N, Leong KF, Wei J. Compressive properties of Ti-6Al-4V lattice structures fabricated by selective laser melting: design, orientation and density. Addit Manuf 2017;16:213–24.
[42] Wauthle R, Vrancken B, Beynaerts B, Jorissen K, Schrooten J, Kruth J-P, Van Humbeeck J. Effects of build orientation and heat treatment on the microstructure and mechanical properties of selective laser melted Ti6Al4V lattice structures. Addit Manuf 2015;5:77–84.
[43] Heinl P, Rottmair A, Körner C, Singer RF. Cellular titanium by selective electron beam melting. Adv Eng Mater 2007;9(5):360–4.
[44] Wang Z, Li Z, Ning J, Zhao L. Effect of heat treatments on the crushing behaviour and energy absorbing performance of aluminium alloy foams. Mater Des 2009;30 (4):977–82.
[45] Dong L, Deshpande V, Wadley H. Mechanical response of Ti–6Al–4V octet-truss lattice structures. Int J Solids Struct 2015;60–61:107–24.
[46] Deshpande VS, Fleck NA, Ashby MF. Effective properties of the octet-turss lattice material. J Mech Phys Solids 2001;49:1747–69.
[47] Al-Ketan O, Abu Al-Rub RK. Multifunctional mechanical metamaterials based on triply periodic minimal surface lattices. Adv Eng Mater 2019;21(10).
[48] Sienkiewicz J, Płatek P, Jiang F, Sun X, Rusinek A. Investigations on the mechanical response of gradient lattice structures manufactured via SLM. Metals 2020;10(2).
[49] Fan H, Hartshorn C, Buchheit T, Tallant D, Assink R, Simpson R, Kissel DJ, Lacks DJ, Torquato S, Brinker CJ. Modulus-density scaling behaviour and framework architecture of nanoporous self-assembled silicas. Nat Mater 2007;6(6): 418–23.
[50] Ashby MF. Hybrids to fill holes in material property space. Philos Mag 2005;85 (26–27):3235–57.
[51] Chen W, Watts S, Jackson JA, Smith WL, Tortorelli DA, Spadaccini CM. Stiff isotropic lattices beyond the Maxwell criterion. Sci Adv 2019;5:eaaw1937.
[52] Razak Z, Sulong ABakar, Muhamad N, Radzi MKhairul Fadzly Md, Ismail NFarhani, Tholibon D, Tharazi I. Numerical simulation analysis of wood/PP composites for injection-moulded car battery trays. Int J Eng Technol 2018;7(3.17).
[53] Kitagawa K, Nakano R. Injection molding defect countermeasures casebook. Seoul: Cmass; 2011.